ONCOIMMUNOLOGY
2025, VOL. 14, NO. 1, 2478850
https://doi.org/10.1080/2162402X.2025.2478850

A targeted MAVS fusion protein for controlled innate immune activation and antitumor therapy

Muhan Wang, Zhijie Zhang, YouYou Yang, Xiaoyi Peng, and Hongping Yin

School of Life Science and Technology, China Pharmaceutical University, Nanjing, China

ABSTRACT

Targeted therapies leveraging the innate immune system are emerging as promising cancer treatments. The mitochondrial antiviral signaling protein (MAVS) plays a crucial role in initiating innate immune responses, but its clinical use is limited by the risk of uncontrolled activation and systemic toxicity. To address this, we developed a novel therapeutic agent, the truncated interferon activation switch (TRIAS), combining MAVS truncates with a tumor antigen-targeting single-chain variable fragment (scFv). This design ensures antigen-dependent, controlled activation. Lentiviral delivery of TRIAS induced significant antitumor responses, including complete tumor regression in some cases. Flow cytometry (FCM) analysis further confirmed that tumor cells were the predominant population expressing the transgene. TRIAS-expressing tumor cells exhibited enhanced antitumor activity, likely due to increased cytokine release and upregulated major histocompatibility complex (MHC) expression, enabling tumor cells to function as antigen-presenting cells. This activated other immune cells, driving adaptive immune responses. Additionally, TRIAS promoted a proinflammatory shift in the tumor microenvironment (TME). In conclusion, TRIAS was validated as an innovative immunotherapeutic agent with MAVS-like immune-activating properties and tightly controlled mechanisms, offering a safer and more effective approach for clinical cancer immunotherapy.

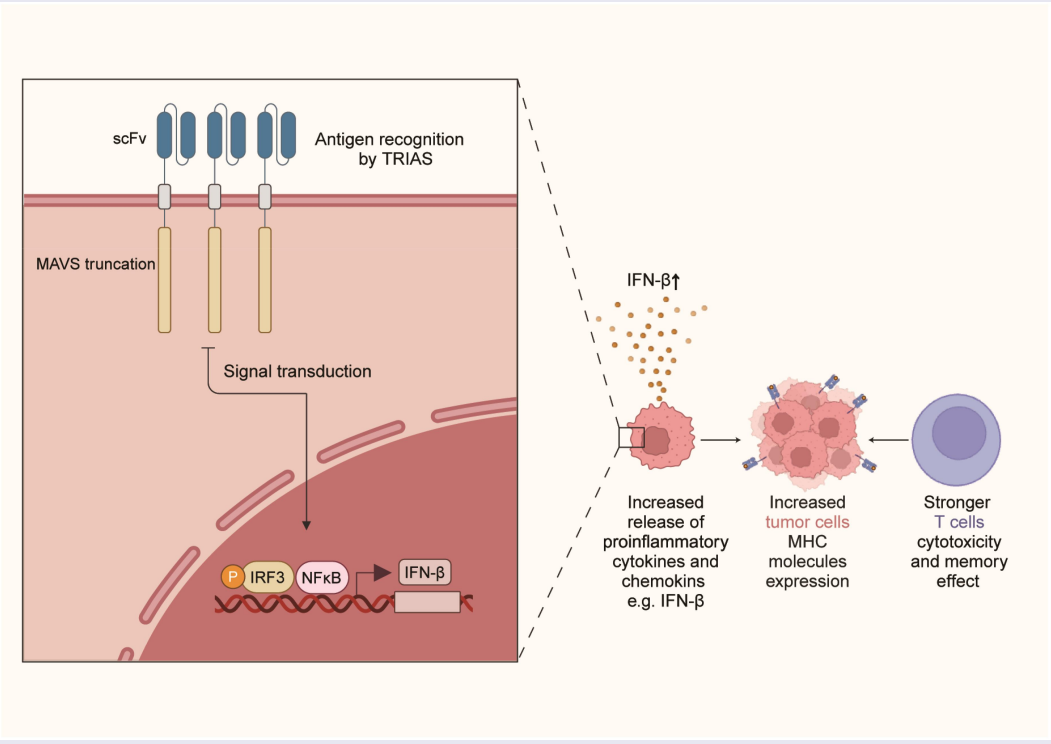

ARTICLE HISTORY
Received 22 January 2025
Revised 25 February 2025
Accepted 6 March 2025

KEYWORDS
Immunotherapy; innate immunity; MAVS; type I interferon; targeted therapy

Introduction

Colorectal cancer (CRC) continues to be a major contributor to cancer-related deaths on a global scale.[1] While immunotherapy, particularly immune checkpoint inhibitors (ICIs), has shown significant efficacy in patients with micro-satellite instability-high (MSI-H) or mismatch repair-deficient

CONTACT Hongping Yin yinhongping@cpu.edu.cn School of Life Science and Technology, China Pharmaceutical University, Nanjing, 211198, China
Supplemental data for this article can be accessed online at https://doi.org/10.1080/2162402X.2025.2478850

(dMMR) CRC.[2–4] However, the majority of CRC cases, characterized as microsatellite stable (MSS) or mismatch repair-proficient (pMMR), remain resistant to such therapies,[5] highlighting the need for alternative or complementary immunotherapeutic approaches.

Recent studies have explored the potential of activating innate immunity to overcome the immune evasion commonly observed in CRC. The innate immune system functions as the first line of defense against pathogens and tumor cells and plays a crucial role in shaping adaptive immune responses.[6] Various preclinical and clinical investigations have demonstrated that innate immune activation can potentiate antitumor immunity in CRC.[7] For example, agonists targeting pattern recognition receptors (PRRs), such as Toll-like receptors (TLRs), RIG-I-like receptors (RLRs), and STING, have been shown to increase dendritic cell maturation, increase type I interferon production, and activate cytotoxic T lymphocytes in mouse models of CRC.[8,9] These findings underscore the importance of targeting innate immunity as an effective therapeutic strategy for CRC.

MAVS is a central adaptor in the RLR pathway, playing a pivotal role in the innate immune defense against RNA viruses.[10] It orchestrates the signal transduction of NF-κB and interferon regulatory factor (IRF) 3/7 signaling, followed by increased production of type I IFNs and other proinflammatory cytokines.[11] Notably, downstream cytokines such as IFN-β have demonstrated significant antitumor effects in preclinical CRC models, including disrupting cell cycle progression, reducing vascularization of liver metastases and inducing apoptosis.[12–15] Furthermore, type I IFNs enhance antigen presentation and promote antitumor immune cell functions such as dendritic cell activation, M1 macrophage polarization, and CD8+ T cell cytotoxicity while inhibiting regulatory T cells (Tregs) and myeloid-derived suppressor cells (MDSCs).[16,17] Analysis of The Cancer Genome Atlas (TCGA) revealed that MAVS expression and the type I IFN pathway are significantly downregulated in various solid tumors, including CRCs.[18] The overexpression of MAVS in colorectal cancer cells has been shown to restore type I IFN signaling, stimulate systemic tumor antigen-specific immune responses and enhance ICI responsiveness, highlighting its potential as a therapeutic target in cancer immunotherapy.[18]

Given the emerging evidence linking MAVS to antitumor immunity, further investigations are warranted to harness its potential in CRC therapy. To achieve precise and controllable immunostimulatory activity through MAVS signaling, we developed a novel immune activation molecule termed TRIAS. Our preclinical studies demonstrated the efficacy of the lentivirus (LVs) encoding TRIAS delivered intravenously (i.v.), which achieved significant tumor inhibition while avoiding the severe toxicity associated with systemic MAVS activation. The greatest efficacy was achieved via the intratumoral (i.t.) delivery route, which demonstrated that the activation of TRIAS within tumor sites evoked strong antitumor effects and led to complete tumor regression. To broaden the application scope, tumor cells were engineered to express TRIAS, which showed robust antitumor efficacy. Mechanistic investigations revealed that TRIAS-mediated efficacy was driven by enhanced MHC molecule expression and the release of proinflammatory cytokines, which collectively amplified immune responses within the tumor microenvironment. These findings position TRIAS as a promising therapeutic strategy with tightly regulated immune activation, offering a novel and effective approach for the treatment of CRC.

Materials and methods

Cell lines

The mouse CT26 colon cancer cell line (RRID: CVCL_7254) were purchased from Cellcook Biotech Company (Guangzhou, China) and cultured in RPMI 1640 media supplemented with 10% FBS and 1× penicillin–streptomycin. The mouse MC38 colon cancer cell line (RRID: CVCL_B288) was purchased from Cyagen Biosciences (Suzhou, China) cultured in DMEM media supplemented with both 10% FBS, 1× penicillin–streptomycin and 1× non-essential amino acids. The mouse LLC Lewis lung carcinoma cell line (RRID: CVCL_4358) were purchased from Cellcook Biotech Company (Guangzhou, China) and cultured in DMEM (modified) media supplemented with 10% FBS and 1× penicillin-streptomycin. The human embryonic kidney HEK293T cell line (RRID: CVCL_0063) was purchased from Procell Life Science & Technology Company (Wuhan, China) and cultured in DMEM media supplemented with 10% FBS and 1× penicillin–streptomycin. All experiments were performed with mycoplasma-free cells.

Construction of lentiviral plasmid

To generate the lentivirus, the GFP, MAVS and TRIAS constructs were inserted into a third generation pTRPE lentiviral backbone with expression driven by an EF1α promoter using standard molecular cloning techniques. The anti-EDB-FN-specific single-chain variable fragment (scFv), L19-scFv, was derived from the human EDB antibody L19[19] (GenBank accession: AJ006113.2). The TRIAS construct was designed to include the L19-scFv, a $(GGGGS)_3$ linker, the CD8 hinge, a CD8 transmembrane domain, and a truncated MAVS intracellular domain. The lentiviral vector express MAVS or TRIAS linked to a GFP-expressing sequence via a P2A element. Lentivirus packaging was performed in HEK293T cells. Briefly, HEK293T cells were co-transfected with the packaging plasmids pLP1, pLP2, and the envelope plasmid pVSV-G using 293 ExpiFectamine (Thermo Fisher Scientific, A14525). The supernatants containing viral particles were collected 48 hours post-transfection and concentrated using the Lenti-X™ Concentrator (Takara 631,232).

Determination of the virus titer

Lentiviruses encoding luciferase, GFP, MAVS or TRIAS were produced via co-transfection of the packaging and envelope plasmids pLP1, pLP2, and pVSV-G into HEK293T cells.[20] The titer of the lentiviral vectors was determined using the serial dilution method in MC38 cells and calculated with the following formula: titer (TU/mL) = (% of cells successfully infected) ×

(total cell count per well) × (dilution factor)]/(volume of inoculum added to cells).

In vivo imaging

Luciferase (Luc) signals in vivo were detected through bioluminescence imaging (BLI) with the IVIS Spectrum In Vivo Imaging System (Perkin Elmer) and analyzed with Living Image 4.5 (PerkinElmer).[21] D-Luciferin (Yeasen, 40902ES03) in 100 μL of PBS was intraperitoneally (i.p.) injected, and after 10 min, the mice were imaged with an exposure time of 10 min. To assess the anatomical distribution of protein expression after intravenous injection of LVs, the mice bearing CT26 tumors were implanted with LVs_Luc via tail vein, and the Luc expression was examined at different indicated time after lentivirus injection. For imaging of the therapeutic model of MC38 tumor cells, the Luc signals of the tumor cells were examined weekly.

Manufacture of TRIAS MC38 cells

MC38 cells were transduced with lentiviruses encoding MAVS or TRIAS. High-purity positive cells were sorted via fluorescence-activated cell sorting (FACS), and the expression of MAVS and TRIAS was confirmed via flow cytometry.

Detection of IFN-β release

For the self-activation assay, MC38 cells were lentivirally transduced with MAVS or TRIAS, release of IFN-β in the culture media was detected via an IFN-β (ABclonal, RK00420) ELISA kit at the indicated time. For the antigen stimulation assay, untransduced (UTD), MAVS or TRIAS MC38 cells were treated with 2 μg/mL EDB-his protein (96-well plate, 200 μL/well). After 48 hours of stimulation, the cell culture supernatants were collected to measure IFN-β release.

Immunoblotting (IB) analysis of phosphorylation

TRIAS MC38 cells were stimulated by 2 μg/mL EDB-his protein for 0, 2, 4 and 6 hours. At the indicated time points, cell lysates were collected and lysed using RIPA buffer (Yeasen, 20101ES60) with protease inhibitors (Yeasen, 20124ES03) and phosphatase inhibitors (Yeasen, 20109ES05). The IB assay was conducted using standard SDS-PAGE technique. The antibodies used in these experiments were as follows: NF-κB p65/RelA Rabbit mAb (ABclonal, A19653), phospho-NF-κB p65 (C22B4) Rabbit mAb (CST, 3033S), IRF-3 Rabbit mAb (ABclonal, A19717), and phospho-IRF-3 (Ser396) (4D4G) Rabbit mAb (CST, 4947S). The membranes were incubated with Immobilon Western Chemiluminescent HRP Substrate (Millipore, WBKLS0500) for signal detection. The signals from the blots were detected with a Tanon 4600SF Chemiluminescent Imaging System.

CCK-8 assay

TRIAS MC38 cells were seeded in 96-well culture plates and incubated with varying concentrations of EDB-his for 24 hours. Afterward, 10 μL of CCK-8 solution (Yeasen, 40203ES76) was added to each well, and cell viability was assessed using a microplate reader at 450 nm.

Detection of MHC molecules expression on tumor cells

UTD, GFP or TRIAS MC38 cells were treated with 2 μg/mL EDB-his protein for 24 hours, the expression of MHC molecules was detected by FCM using APC-conjugated anti-mouse H-2Kb antibodies (Biolegend 116,517) and PerCP-conjugated anti-mouse MHC II (I-A/I-E) antibodies (Elabscience, E-AB-F0990F).

FCM analysis of intratumoral GFP-expressing cells

1×10^6 mCherry-MC38 cells were implanted subcutaneously into the flanks of C57BL/6 mice, 1×10^6 TU LVs_GFP were inoculated intratumorally at 5 days after initial implantation every 3 days for three times. One day after the last injection, whole tumors tissues were collected, minced into fragments smaller than 1 mm, and digested with 100 μg/mL collagenase I and 75 μg/mL DNAse I for 1 hour at 37°C. The mixture was passed with a 70-μm filter and red blood cells were eliminated by incubation with ACK Lysis Buffer (Yuanye, R20172). The cells were stained with fluorochrome-conjugated Abs in PBS containing 2% FBS for 30 min at 4°C after blockade with purified rat anti-mouse CD16/CD32 (Mouse BD Fc Block) (2.4G2) (BD 553,141). The following Abs were used: Fixable Viability Stain 780 (BD 565,388) and Alexa Fluor 700 rat anti-mouse CD45 (30-F11) (BD 560,510). Data acquisition was performed using an LSR flow cytometer (BD Biosciences), and the results were analyzed with FlowJo software (version 9).

Measurement of cytokine in the tumor tissue

Tumor tissue was homogenized with a tissue homogenizer in ice-cold RIPA lysis buffer supplemented with protease inhibitor (Yeasen, 20124ES03). Intratumoral cytokines in MC38 tumor models were quantified via an IFN-β (ABclonal, RK00420) ELISA kit. The concentrations of cytokines in the tumor lysates were standardized to the total protein of each sample, which was measured via a BCA protein assay kit (Beyotime, P0011).

Mouse models

Female BALB/c mice and C57BL/6 mice aged 6–8 weeks were purchased from Aniphe BioLab (Nanjing, China) and housed under SPF conditions at China Pharmaceutical University. For evaluation of in vivo efficacy of LVs_TRIAS, tumor models were established via the subcutaneous injection of 5×10^5 CT26 cells into BALB/c mice or 1×10^6 MC38 cells into C57BL/6 mice. The tumor volume was determined via the following formula: $V = (L \times W \times W)/2$, where V represents the tumor volume, W is the tumor width, and L is the tumor length. The mice were considered to have reached humane endpoints if their body weight decreased by more than 15% or if their tumor volume exceeded 1000 mm^3. The animals were euthanized following

the ethical guidelines for animal experimentation. For the lentivirus treatment model, the mice were randomized on the basis of tumor size and stratified into treatment groups at 5 days after tumor cell implantation. Tumor volume and body weight were measured every 3–4 days. For intravenous delivery, a single dose of 1×10^7 TU of LVs_GFP, LVs_MAVS or LVs_TRIAS was injected via the tail vein ($n = 5$). For intratumoral delivery, lentivirus was delivered every 3 days for three times ($n = 5$). After 1 month, the mice with complete tumor regression and age-matched naïve mice were challenged with 1×10^6 MC38 cells in the left flank and 5×10^5 LLC cells in the right flank. For the therapeutic tumor vaccine model, mice were randomized into treatment groups based on tumor size 5 days after the initial implantation of tumor cells, and stratified into treatment groups of MAVS MC38 cells or TRIAS MC38 cells ($n = 5$). Tumor growth was monitored by in vivo bioluminescence imaging every week.

Immunohistochemistry (IHC) analysis

A total of 5×10^5 CT26 cells were injected subcutaneously into BALB/c mice, and 1×10^6 MC38 cells were injected subcutaneously into C57BL/6 mice. Different volumes of tumor tissues were collected, and EDB expression was detected by IHC with an L19 antibody.

Bulk RNA sequencing (RNAseq)

1×10^6 MC38 cells were implanted subcutaneously into the flanks of C57BL/6 mice, saline or 1×10^6 MAVS MC38 cells or TRIAS MC38 cells were inoculated intravenously at 5 days after initial implantation. Tumor tissues were resected 7 days after the treatment. Library preparation and Illumina sequencing were conducted at GENEWIZ Co. Ltd. (Suzhou, China) using 1 μg of total RNA from every group. Gene and isoform expression levels were estimated using HTSeq (V.0.6.1) from the paired-end cleaned data. Differential expression analysis was conducted with the edgeR (V3.28.1) Bioconductor package, based on a negative binomial distribution model. Dispersion estimates and logarithmic fold changes in gene expression were derived from data-driven prior distributions. A significance threshold for gene expression differences (Padj) was set at < 0.05. The volcano plot was created using the R package EnhancedVolcano (V.1.16), and the heatmap was generated using Complexheatmap (V.2.16.0) after normalizing and scaling the data within each specified gene set. Normalized counts from DESeq2 were used for analysis with GSEA.

Statistical analysis

For the comparison of multiple groups, one-way or two-way analysis of variance (ANOVA) was employed. Kaplan-Meier curves were utilized to graphically represent the in vivo survival data and the log-rank test was implemented to ascertain the differences between the groups.

Results

Construction of TRIAS with inducible activity

Given that MAVS plays a crucial role in immune stimulation, we first injected a lentivirus encoding MAVS (LVs_MAVS) via tail vein using a subcutaneous CT26 tumor model. Notably, a single dose of LVs_MAVS administration led to severe toxicity with piloerection, eye inflammation and significant body weight loss compared with those of the control group (Supplementary Figure S1). This finding suggests that systemic activation of MAVS signaling is deleterious to the body, corresponding with the clinical toxicity associated with IFN-β administration.[22] To address this challenge, we developed a switchable MAVS variant designed to only activate in the presence of tumor antigens, termed as TRIAS. TRIAS lacks the mitochondrial membrane domain and incorporates a tumor antigen-specific scFv along with a cytoplasmic transmembrane domain at its N-terminus (Figure 1a). Previous research has demonstrated that the fibronectin (Fn) variant extra domain B (EDB) is exclusively expressed in processes such as embryonic development or tumor angiogenesis.[23,24] This restricted expression makes EDB-fibronectin an attractive target.[25] Furthermore, type I IFNs are known to inhibit angiogenesis, providing a complementary mechanism for targeting the tumor vasculature.[26,27] On the basis of these properties, L19 scFv, an antibody fragment with high specificity for EDB-fibronectin, was chosen for its potential to adapt this design.

To characterize the functionality of TRIAS, we compared the downstream IFN-β signaling dynamics of TRIAS and MAVS in MC38 cells over 96 hours post-transduction (Figure 1(c)). The overexpression of MAVS in cells triggered autonomous IFN-β release, with activity decreasing within 96 hours post-transduction. TRIAS exhibited minimal self-activation within the initial 24 hours (Figure 1(c)). After 96 hours, when IFN-β signaling returned to baseline, antigen stimulation of TRIAS-expressing cells led to significant release of IFN-β (Figure 1(d)). In contrast, MAVS-expressing cells remained inactive, underscoring the antigen-specific and switchable nature of TRIAS activity (Figure 1(d)). To evaluate whether this design exhibited antigen-dependent activity without causing toxicity, the same delivery strategy was also applied with TRIAS in the subcutaneous CT26 tumor model (Figure 1(e)). Tumor growth was suppressed in the TRIAS-treated group, demonstrating its therapeutic potential (Figure 1(f)). Additionally, no significant loss in body weight was observed during the treatment (Figure 1g). The expression of EDB in CT26 tumors was confirmed by IHC (Supplementary Figure S2), and it can be speculated that the activation of TRIAS is localized and occurs exclusively within tumor sites, which aligns with the inducible mechanism of this therapeutic approach. Collectively, these findings indicate that TRIAS exhibits tightly regulated antitumor activity and a favorable safety profile compared with MAVS.

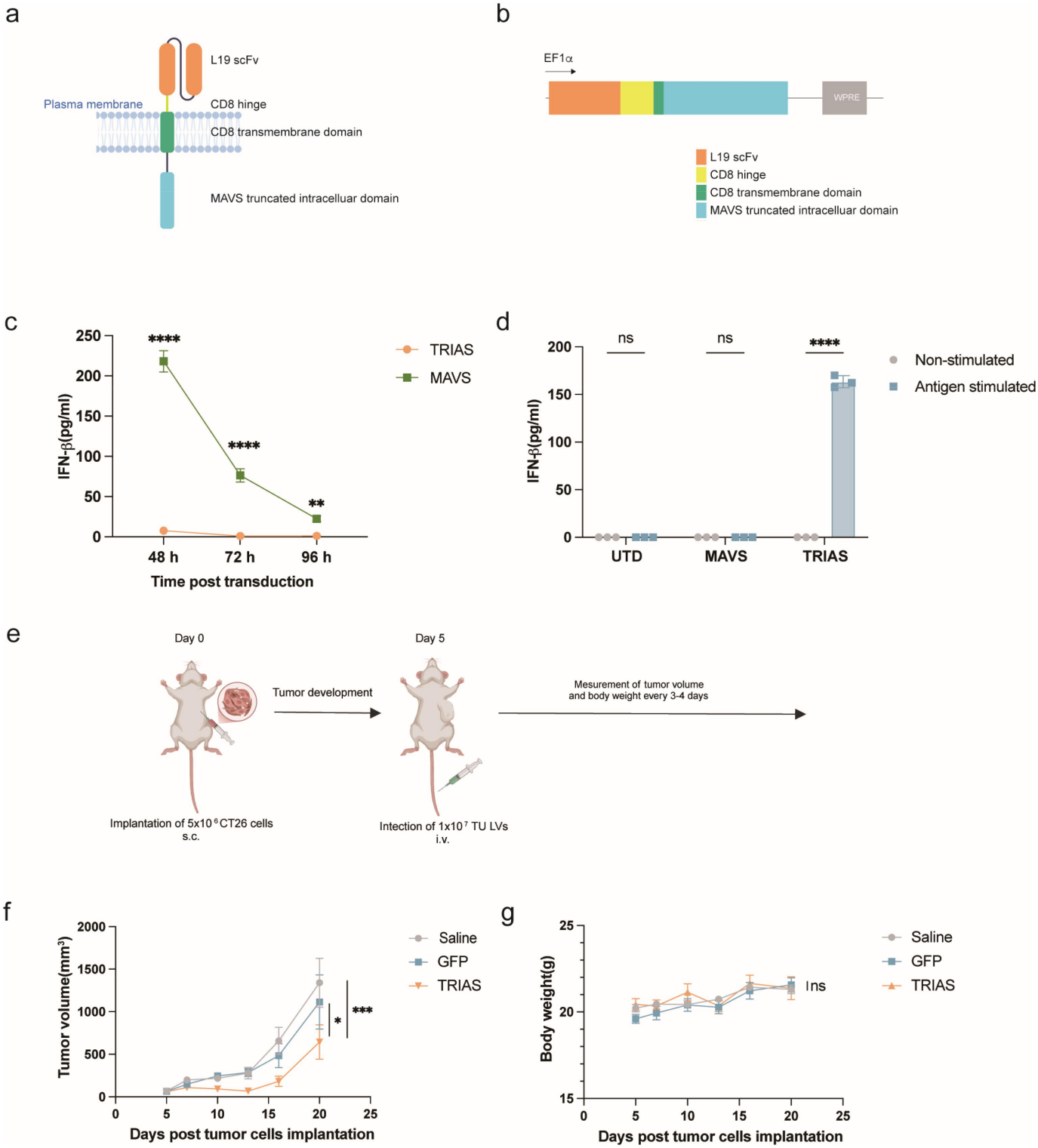

Figure 1. Evaluation of TRIAS activity (a) schematic representation of TRIAS components. TRIAS comprises an L19 scFv, CD8 hinge, CD8 transmembrane domain, and the truncated MAVS intracellular domain. (b) Schematic representation of lentiviral vectors. The lentiviral vectors express TRIAS linked to a gfp-expressing sequence via a P2A element. (c) Monitoring of ifn-β release after the overexpression of MAVS and TRIAS at the indicated time post transduction. Average and standard deviation of triplicate culture wells are shown. p-values were calculated by two-way ANOVA with Tukey's multiple comparison test. $^{**}p < 0.01$; $^{****}p < 0.0001$. (d) Detection of ifn-β release by TRIAS cells upon stimulation with antigens. Average and standard deviation of triplicate culture wells are shown. p-values were calculated by two-way ANOVA with Tukey's multiple comparison test. $^{****}p < 0.0001$; ns, non-significant). (e) Schematic illustration of the CT26 tumor model. BALB/c mice bearing subcutaneous CT26 tumors received a single intravenous injection of 1×10^7 TU LVs on day 5. (f) Tumor growth of different groups. (g) Monitor of body weights during the whole procedure. Average and standard error of the mean of the tumor volume and body weight after treatment with saline, LVs_GFP and LVs_TRIAS ($n = 5$/group) are shown. p-values were calculated by two-way ANOVA with Tukey's multiple comparison test. $^{*}p < 0.5$; $^{***}p < 0.001$; ns, non-significant.

Intratumoral administration of LVs_TRIAS induced complete tumor regression and long-term protection against tumors

In vivo imaging following intravenous injection of LVs_luciferase confirmed successful luciferase expression across cells (Supplementary Figure S3), which supports the efficacy achieved in the intravenous treatment model. However, it demonstrated a lack of tissue specificity despite stronger signals accumulating in the liver (Supplementary Figure S3). The liver bypasses most lentivirus particles,[28] which limits the efficacy of TRIAS via intravenous delivery. To obtain the maximal efficacy of TRIAS, we next evaluated the antitumor effects via intratumoral injection of LVs_TRIAS, ensuring efficient delivery of lentivirus within the tumor sites (Figure 2(a)-i and ii). In CRC immunotherapy research, the two most commonly used immune-competent syngeneic murine models are the CT26[29] and MC38[30] tumor models. Notably, MC38 cells are highly immunogenic with an immune-infiltrated phenotype,[31] whereas CT26 cells are highly undifferentiated and proliferative.[32] To characterize the behavior of TRIAS in different immunological backgrounds, antitumor efficacy was examined in both the CT26 and MC38 tumor models. In the CT26 tumor model, treatment with LVs_TRIAS significantly inhibited the growth of CT26 tumors and prolonged overall survival (Figure 2(b,f)). The MC38 tumor model exhibited superior outcomes, including enhanced tumor suppression and extended survival (Figure 2(c,g)). Notably, two out of five mice in the LVs_TRIAS group achieved complete tumor regression (CR) in the MC38 tumor model (Figure 2(c)). No weight loss was observed in any of the groups during the entire process (Figure 2(d,e)). CR mice were rechallenged with parental MC38 cells and LLC cells to assess the development of tumor-specific immunologic memory responses (Figure 2(a)-iii). The mice that had previously been cured of the tumors completely rejected subsequent MC38 tumor growth, whereas the naïve mice grew tumors with the expected kinetics (Figure 2(h)), it revealed that TRIAS expression-induced innate immune activation led to sustained adaptive immunological memory against the tumors. In addition, the growth of LLC tumors was effectively inhibited in immunized mice compared with that in naïve mice (Figure 2(i)), indicating the development of a systemic antitumor immune response with cross-reactivity. These findings demonstrated that TRIAS activation within tumor sites demonstrated robust antitumor efficacy, achieving complete tumor eradication in certain cases. Additionally, it elicits durable immune memory responses, providing long-term protection against tumor recurrence.

Engineering of TRIAS tumor cells and validation of its immunostimulant activity

To assess the in vivo translation efficiency and identify the cell types involved in lentivirus uptake and translation, we administered a lentivirus encoding GFP intralesionally followed by FCM analysis of GFP+ cells in the tumor tissues. The MC38 cells were tagged using mCherry for better characterization of tumor cells. Our data revealed that tumor cells (mCherry+), leukocytes (CD45+) and stromal cells (mCherry-CD45-) were all able to uptake and translate the injected lentivirus, whereas tumor cells were the dominant population (Supplementary Figure S4). To estimate the function of the expression of TRIAS in tumor cells and broaden the application scenarios, we engineered MC38 cells with TRIAS by lentivirus transduction, and approximately 70% of the cells successfully expressed TRIAS, as detected by flow cytometry (Figure 3(a)). TRIAS shares the same functional domains as MAVS, to test whether the stimulation of TRIAS with specific antigens induces the same signal transduction as MAVS does, the in vitro activity profiles of TRIAS-treated MC38 cells were examined by stimulating the cells with antigens. In vitro stimulation of MC38 cells with antigens demonstrated the phosphorylation of IRF-3 and NF-κB (Figure 3(b)), which was indicative of MAVS downstream signaling, e.g., type I immune response. Type I IFN stimulation has been shown to induce the expression of major histocompatibility complex (MHC) molecules on tumor cells, increasing their immunogenicity.[33] FCM analysis demonstrated that the activation of TRIAS downstream signaling significantly upregulated MHC class I and class II molecule expression in MC38 tumor cells (Figure 3(c)), further supporting its role in antigen presentation. Enhanced IFN-β secretion and upregulation of MHC molecule expression were also observed in CT26 cells (Supplementary Figure S5), indicating that these effects are not restricted to specific cell lines. Moreover, cell viability was suppressed in an antigen concentration-dependent manner (Figure 3(d)). Taken together, these findings suggest that TRIAS-induced tumor cells have antigen-dependent stimulatory effects, with increased production of proinflammatory cytokines, suppression of tumor growth, and increased capacity for antigen presentation. These findings highlight the multifaceted role of TRIAS in mediating robust antitumor immune responses and its potential utility in tumor immunotherapy.

TRIAS tumor cells exhibited significant tumor growth inhibition

Motivated by the in vitro immunostimulatory effects of TRIAS tumor cells, we further evaluated the in vivo antitumor efficacy of TRIAS MC38 cells using a subcutaneous MC38 tumor model as well. To assess the tumor-targeting and specific activation ability of TRIAS, an intravenous treatment model was established to investigate the therapeutic efficacy of TRIAS MC38 cells administered via tail vein injection (Figure 4(a)). Specifically, mice were treated with a single dose of tumor vaccine 5 days after initial tumor cell implantation. TRIAS MC38 cells demonstrated significant tumor inhibition (Figure 4(b,c)), effectively suppressing tumor growth without causing body weight loss (Figure 4(d)). In contrast, no efficacy was observed in the MAVS MC38 cell treatment group (Figure 4b,c), suggesting a loss of MAVS MC38 cell activity during the production process. No weight loss was observed in all groups during the entire process (Figure 4(d)). Collectively, these results underscore the durable activity of TRIAS MC38 cells and its potential as a promising strategy for inducing systemic antitumor immunity.

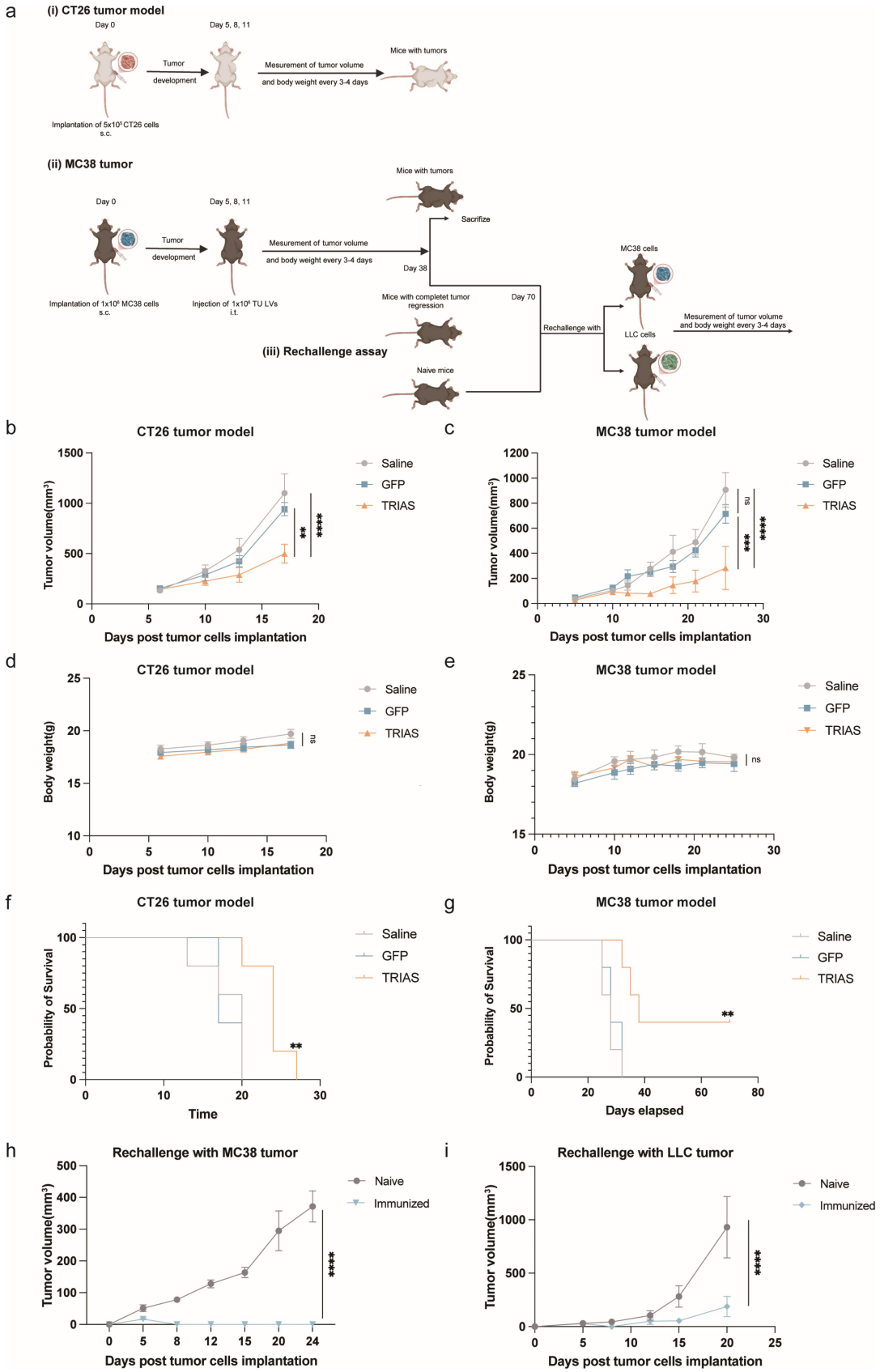

Figure 2. Intratumoral delivery of LVs_TRIAS induced systemic antitumor immunity in vivo (a) schematic illustration of the CT26 and MC38 tumor models. A total of 5×10^5 CT26 cells were implanted into the flanks of BALB/c mice, and 1×10^6 MC38 cells were engrafted into the flanks of C57BL/6 mice. At 5-, 8- and 11-days post-implantation, the tumors were intralesionally challenged with 1×10^6 TU LVs for three times. (b–c) Tumor growth curve with different treatments. (d–e) Body weight curve with different treatments. Average and standard error of the mean of the tumor volumes and body weight after intratumoral treatment with saline, LVs_GFP and LVs_TRIAS ($n = 5$/group) are shown. p-values were calculated by two-way ANOVA with Tukey's multiple comparison test. $^{**}p < 0.01$; $^{***}p < 0.001$; $^{****}p < 0.0001$; ns, non-significant. (f–g) Kaplan–Meier survival curves of different treatment groups. p-values were calculated by Log-rank test. $^{**}p < 0.01$. (h–i) Mice with complete tumor regression from (a-ii) and age-matched naïve mice were challenged with parental MC38 cells or LLC cells, and the tumor volume was measured during the rechallenge assay (naïve $n = 5$ and rechallenge $n = 2$). p-values were calculated by two-way ANOVA with Tukey's multiple comparison test. $^{****}p < 0.0001$.

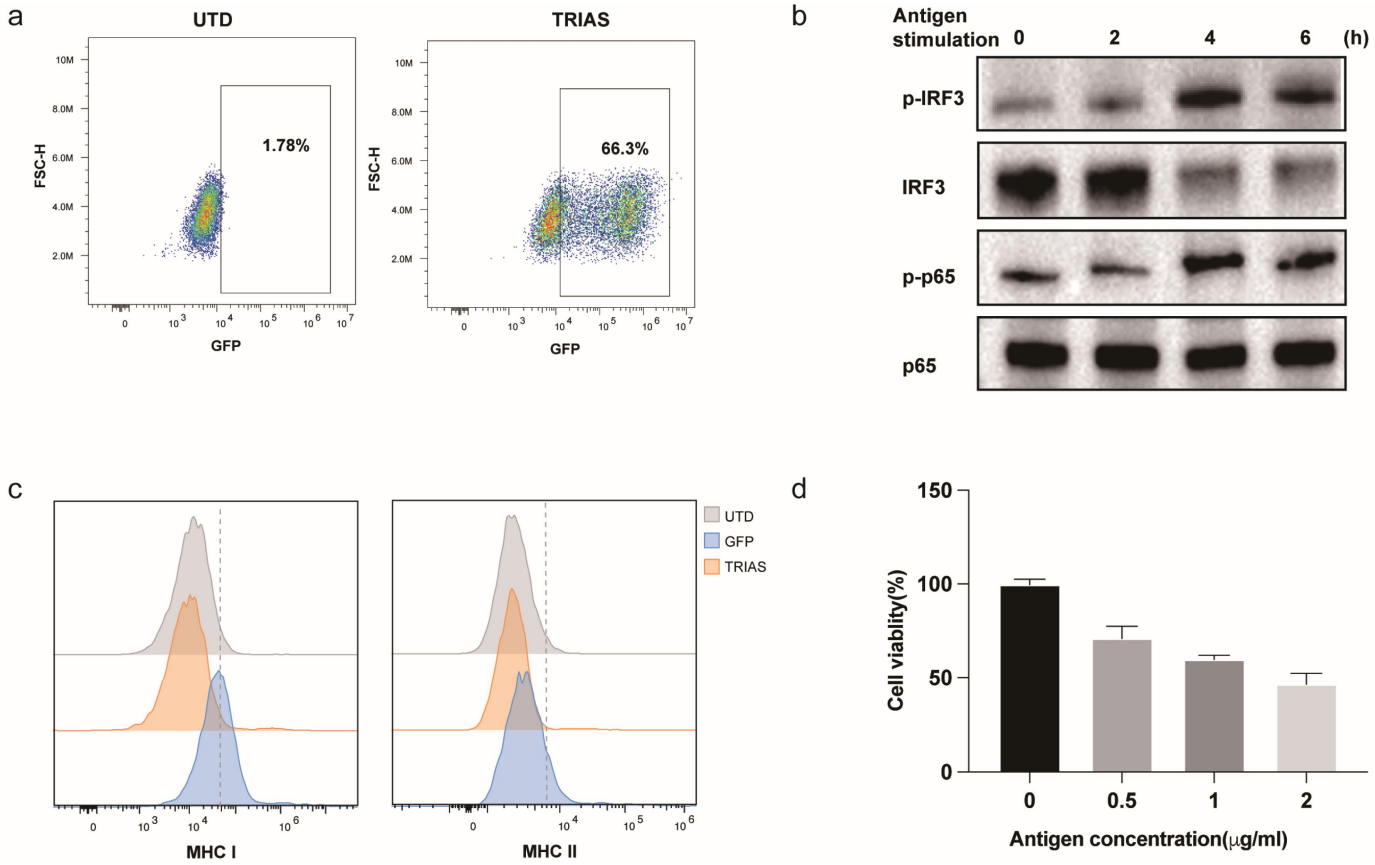

Figure 3. TRIAS expression on tumor cells induced proinflammatory effects (a) the expression of TRIAS in MC38 cells was confirmed by flow cytometry. (b) Cell lysates were collected to detect the phosphorylation levels of IRF-3 and NF-κB following antigen stimulation at the indicated time points. (c) FCM analysis of MHC I and MHC II expression in MC38 cells engineered with different constructions. (d) The viability of the TRIAS cells exposed to different concentrations of antigens was detected by a CCK-8 assay.

Immunization of TRIAS MC38 cells promotes type I IFN signaling and reprograms the TME to a more inflamed state

To validate the specific activation of TRIAS MC38 cells upon recognition of antigens, we investigated whether the concentration of cytokines was effectively enriched within tumors and observed a significant increase of IFN-β levels compared with those in the control group (Figure 5(a)). We then performed multicolor flow cytometry to detect the infiltration of immune cells within the tumor tissue and found a greater portion of CD45+ leukocytes accumulated in the tumor tissue (Figure 5(b)). To gain deeper insight into the immune responses triggered by the TRIAS tumor cells, we performed RNA sequencing on samples extracted from tumor tissues collected 7 days post-treatment. Pairwise differential gene expression analysis revealed 1141 differentially expressed genes (DEGs; 546 upregulated and 595 downregulated) (Figure 5(c)).

Consistent with the in vivo anti-tumor activity assay, treatment with MAVS MC38 cells failed to elicit immune responses. (Figure 5(a,b,d)). A comparison of the IFN regulation signature expression revealed that tumor tissues treated with TRIAS MC38 cells had significantly greater type I IFN signaling activity than did the control group (Figure 5(d)). To characterize the immune-related pathways affected by TRIAS in MC38 cells, we performed gene set enrichment analysis (GSEA) via the Kyoto Encyclopedia of Genes and Genomes (KEGG) database. The GSEA results demonstrated significant upregulation of multiple inflammation-related pathways, including the TNF signaling pathway, Toll-like receptor signaling pathway, NF-κB signaling pathway and RIG-I-like receptor signaling pathway, as well as immune activation pathways, such as cytokine-cytokine receptor interaction, chemokine signaling pathway, T-cell receptor signaling pathway, and JAK-STAT signaling pathway, in the TRIAS group compared to the control group (Figure 5(e)). These pathways are closely associated with type I IFN signaling. For example, type I IFN production is activated in the TLR signaling pathway and the RLR signaling pathway through the induction of IRFs and NF-κB. Additionally, The JAK-STAT signaling pathway is a central downstream effector of type I IFN signaling, mediating the transcriptional activation of interferon-stimulated genes (ISGs). Taken together, the findings from ELISA of cytokine production, FCM analysis of immune infiltration and RNA-seq data suggest that TRIAS MC38 cells induce an antitumor response by specifically releasing proinflammatory cytokines, recruiting immune cells and promoting proinflammatory events.

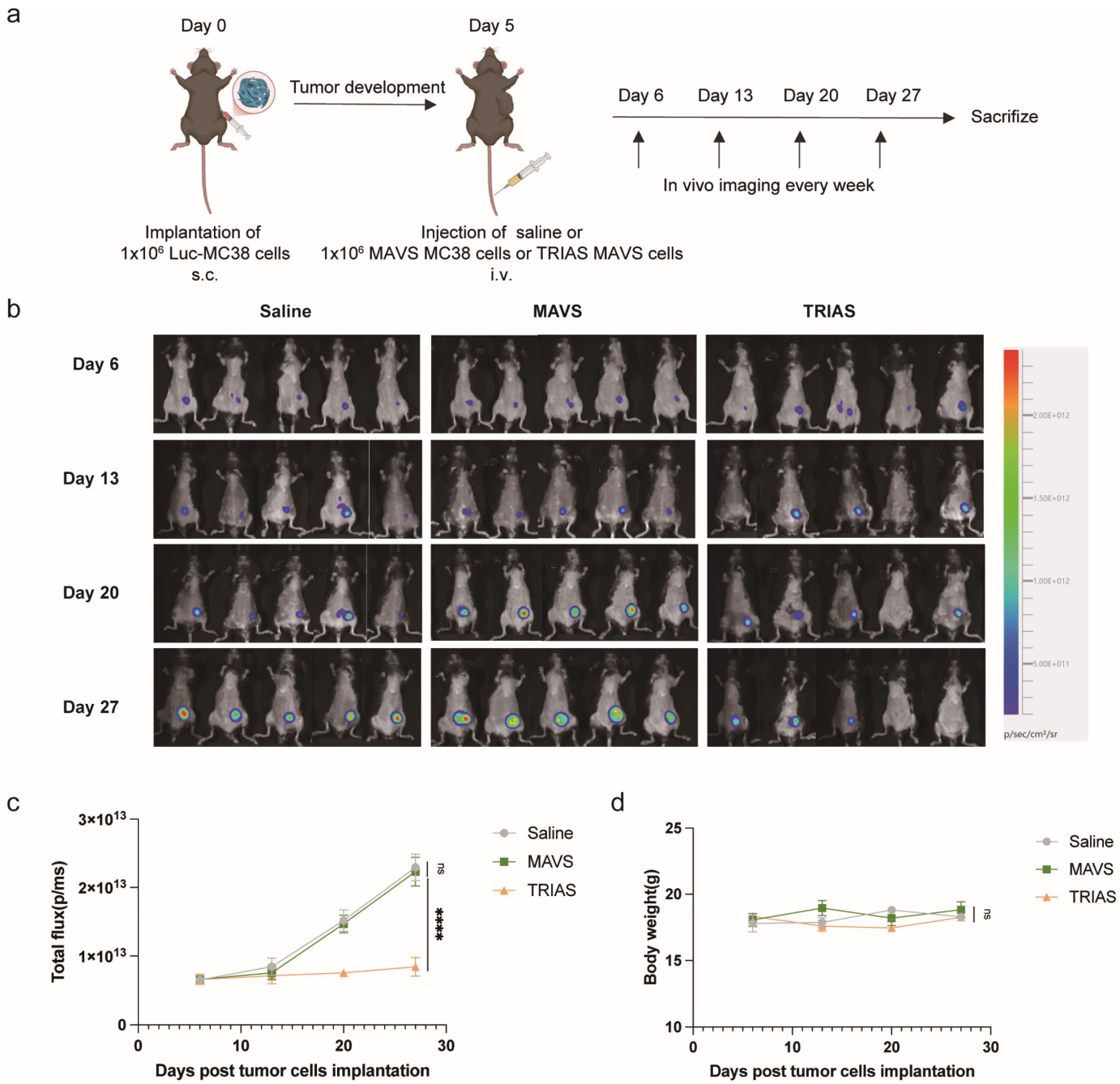

Figure 4. TRIAS MC38 cells have robust antitumor effects (a) schematic illustration of the MC38 tumor model. 1×10^6 luc-MC38 cells were implanted into the flanks of C57BL/6 mice, 1×10^6 saline, MAVS MC38 cells or TIIAR MC38 cells were inoculated via the tail vein at 5 days after initial implantation. In vivo bioluminescence imaging was performed every week. (b) Monitoring of in vivo bioluminescence signals at the indicated time. (c) Statistical analysis of bioluminescence of different groups. (d) Body weight curve with different treatment. Average and standard error of the mean of the bioluminescence and body weight after treatment with saline, MAVS MC38 cells and TRIAS MC38 cells ($n = 5$/group) are shown. p-values were calculated by two-way ANOVA with Tukey's multiple comparison test. ****$p < 0.0001$; ns, non-significant.

Discussion

Evidence from clinical trials and preclinical studies highlights the intricate relationship between the innate immune system and adaptive immune responses.[7] The activation of the innate immune system allows for sustained effector lymphocyte-mediated tumor cell killing, thereby bridging innate immunity with long-term adaptive immune protection.[34] MAVS is a crucial adaptor in the innate immunity and local overexpression of MAVS has been shown to enhance CD8+ T-cell-mediated antitumor immunity, highlighting its therapeutic potential.[18] However, intratumoral delivery of MAVS faces significant challenges in clinical applications because of the location and accessibility of tumors. CRC tumors are often located deep within the abdominal cavity or the rectum, making them less accessible for direct intralesional injection without advanced imaging or invasive procedures. To address these limitations, we investigated the possibility of delivering LVs_MAVS by intravenous injection but it demonstrated the associated toxicity of widespread MAVS expression

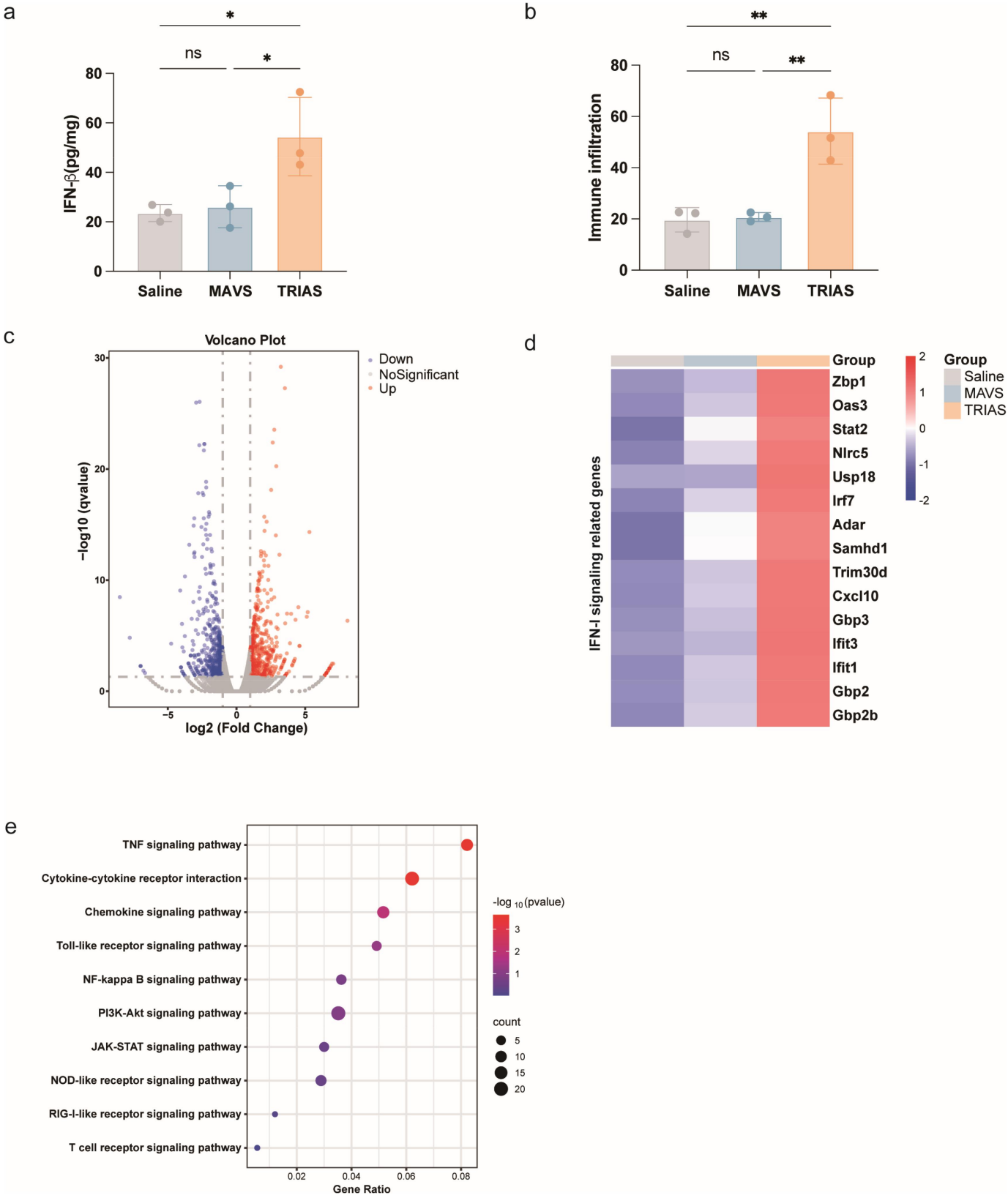

Figure 5. TRIAS MC38 cells reprogrammed the TME to a more proinflammatory state (a) release of ifn-β in tumors at 48 h post-treatment was measured by ELISA. Average and standard deviation of triplicate culture wells are shown. p-values were calculated by two-way ANOVA with Tukey's multiple comparison test. *$p < 0.5$; ns, non-significant. (b) 1 week after treatment, the treated tumors were collected and analyzed by FCM to calculate the percentages of infiltrating CD45+ leukocytes in MC38 tumors. Average and standard deviation of percentage of infiltrated CD45+ cells among total live cells are shown ($n = 3$/group). p-values were calculated by two-way ANOVA with Tukey's multiple comparison test. ****$p < 0.0001$; ns, non-significant. (c) Volcano plots demonstrating the upregulated and downregulated differentially expressed genes (DEGs) in the TRIAS group compared with the control group. (d) Heatmap of the expression of genes associated with IFN-I signaling. (e) KEGG analysis of the enrichment of proinflammatory pathways in the TRIAS group.

(Supplementary Figure S1). This prompted the design of a novel, controllable interferon activation switch, termed TRIAS (Figure 1(b)). The tightly regulated activity of TRIAS was proved both in vitro (Figure 1(d)) and in vivo (Figure 1f).

FCM analysis of intratumoral cells following LVs_GFP injection revealed that GFP expression was predominantly observed in tumor cells (Supplementary Figure S4). Based on the significant antitumor efficacy demonstrated by LVs_TRIAS (Figure 2), it is plausible that tumor cells expressing TRIAS play a critical immunomodulatory role within the tumor microenvironment. Therapeutic tumor cells represent a promising approach in cancer treatment because of their capacity to act as a natural source of neoantigens.[35] They are typically inactivated through lysis or irradiation prior to administration to enhance immunogenicity, which stimulates immune infiltration to the tumor site with strong antitumor immune response.[36] Unlike inactivated tumor cells, living tumor cells possess unique characteristics of tumor homing.[37–40] Despite of these characteristics, there are several advantages of engineering tumor cells with TRIAS. First, tumor cells can act as "Trojan horses" for therapeutic delivery, as their native tumor-tropic ability, combined with targeted antigen recognition mediated by engineered scFv molecules of TRIAS, ensures the precise delivery of immune responses within the tumor microenvironment. Furthermore, tumor cells, particularly patient-specific autologous tumor cells, serve as a source of neoantigens, which can potentially promote antigen-specific T-cell immunity targeting the tumor.[35]

The limited efficacy observed with MAVS MC38 cells, in contrast to the robust antitumor activity of TRIAS cells, can be attributed to several key factors. First, MAVS cells lack the controlled activation mechanism inherent to TRIAS. As demonstrated in Figure 1(c,d), MAVS MC38 cells initiated cytokine release immediately after transduction, but this response diminished by 96 hours, likely due to pathway exhaustion or desensitization. In contrast, TRIAS MC38 cells exhibited sustained activation, as their response was tightly regulated by tumor-associated antigens, ensuring prolonged and targeted immune stimulation. In addition, while tumor cells possess intrinsic homing capabilities, the incorporation of the L19 scFv domain in TRIAS enhances tumor targeting. This allows a greater number of TRIAS cells to traffic to tumor sites, amplifying the immune response. MAVS cells, however, lack this targeting ability, and their activity may be diluted in the bloodstream before reaching the tumor microenvironment. This is further supported by Figure 5(a), where IFN-β levels were significantly elevated only in the TRIAS-treated group, while the MAVS group showed levels comparable to the control group. Collectively, these findings underscore the critical advantages of TRIAS, including its antigen-dependent activation and enhanced tumor targeting, which synergistically contribute to its superior antitumor efficacy. This highlights the importance of precise immune modulation in achieving effective cancer immunotherapy.

Recent studies have demonstrated the efficacy of engineered tumor cells that secrete immunomodulatory agents such as IFN-β and GM-CSF in achieving efficient tumor eradication.[36] In this study, TRIAS activation triggered IRF-3 and NF-κB phosphorylation, leading to the release of IFN-β (Figure 5(b)) along with other pro-inflammatory cytokines and chemokines. Therefore, the immune response of TRIAS tumor cells could further be amplified by the addition of these immunostimulants.

In immune responses to specific antigens, major histocompatibility complexes (MHC-I and MHC-II) are critical for targeting and presenting antigens, both within cells and from external pathogens.[41] The downregulation of MHC-I has been described in numerous tumor types and is often tightly associated with immune evasion.[41] IFNs have been shown to counteract this by restoring MHC-I expression and enhancing antigen processing.[42] In addition, MHC II molecules are often expressed on professional APCs, which are mainly dendritic cells, whereas several studies have attempted to express MHC-II molecules on tumor cells by transfection of class II major histocompatibility complex transactivator (CIITA) to make tumor cells highly immunogenic and therefore induce a protective CD4+ T-cell response.[43,44] Our study revealed that stimulation with TRIAS upregulated the expression of both MHC-I and MHC-II molecules on tumor cells (Figure 3(c)). This dual upregulation suggests a potential mechanism for TRIAS-mediated antitumor efficacy by enhancing T-cell recognition, thereby bolstering both CD8+ and CD4+ T-cell responses against tumor cells.

In conclusion, our investigation highlights that TRIAS has advantages over MAVS, with specific and controllable activity without inducing systemic toxicity. Notably, the intratumoral expression of TRIAS triggered potent antitumor effects with partial complete tumor regression. Furthermore, FCM analysis of single-cell suspensions from tumor tissues revealed that tumor cells were the dominant population that expressed TRIAS after lentivirus injection, which underscores the possible activity mechanism of TRIAS. Additionally, to broaden the therapeutic potential, we investigated TRIAS-expressing tumor cells functionalities and found that they exhibited enhanced antitumor efficacy, likely through the upregulation of MHC class I and II molecules, enabling them to function as nonprofessional antigen-presenting cells. Collectively, these findings suggest that TRIAS, which has MAVS-like immunostimulatory activity and an antigen-dependent "on switch" mechanism, may be a promising targeted therapeutic strategy for clinical immunotherapy applications.

Acknowledgments

All schematics were created using BioRender with a license.

Author contributions

CRediT: **Muhan Wang:** Conceptualization, Investigation, Methodology, Validation, Writing – original draft, Writing – review & editing; **Zhijie Zhang:** Funding acquisition, Writing – review & editing; **YouYou Yang:** Investigation, Validation; **Xiaoyi Peng:** Investigation, Validation; **Hongping Yin:** Funding acquisition, Supervision, Writing – review & editing.

Disclosure statement

MW, XP, YY, ZZ and HY are listed as inventors on corresponding patent.

Funding

This study was supported by grants from Jiangsu Funding Program for Excellent Postdoctoral Talent [No. 2023ZB409] and Postdoctoral Fellowship Program of CPSF [No. GZC20233117].

ARRIVE guidelines

The study adheres to ARRIVE guidelines. A completed ARRIVE checklist is provided in the supplementary materials for this manuscript.

Author contributions

TRIAS was designed by MW and evaluated by MW, YY and XP. MW contributed to analysis and interpretation of results. The manuscript was written by MW and edited by ZZ. The financial support came from funds of ZZ and HY. This work was under supervision of HY. All authors reviewed the manuscript.

Data availability statement

Sequencing data is available from the corresponding author upon request.

Ethics approval

The Institutional Animal Care and Use Committee of China Pharmaceutical University reviewed and approved all experimental animal protocols with a protocol identification number 2023-06-037.

References

1. Sahin IH, Akce M, Alese O, Shaib W, Lesinski GB, El-Rayes B, Wu C. Immune checkpoint inhibitors for the treatment of MSI-H/MMR-D colorectal cancer and a perspective on resistance mechanisms. Br J Cancer. 2019;121(10):809–818. doi: 10.1038/s41416-019-0599-y.
2. Siegel RL, Wagle NS, Cercek A, Smith RA, Jemal A. Colorectal cancer statistics, 2023. CA Cancer J Clin. 2023;73(3):233–254. doi: 10.3322/caac.21772.
3. Le DT, Uram JN, Wang H, Bartlett BR, Kemberling H, Eyring AD, Skora AD, Luber BS, Azad NS, Laheru D, et al. PD-1 blockade in tumors with mismatch-repair deficiency. N Engl J Med. 2015;372(26):2509–2520. doi: 10.1056/NEJMoa1500596.
4. Le DT, Durham JN, Smith KN, Wang H, Bartlett BR, Aulakh LK, Lu S, Kemberling H, Wilt C, Luber BS, et al. Mismatch-repair deficiency predicts response of solid tumors to PD-1 blockade. Science. 2017;357(6349):409–413. doi: 10.1126/science.aan6733.
5. Ganesh K, Stadler ZK, Cercek A, Mendelsohn RB, Shia J, Segal NH, Diaz LA. Immunotherapy in colorectal cancer: rationale, challenges and potential. Nat Rev Gastroenterol Hepatol. 2019;16(6):361–375. doi: 10.1038/s41575-019-0126-x.
6. Li X, Dai H, Wang H, Han W. Exploring innate immunity in cancer immunotherapy: opportunities and challenges. Cell Mol Immunol. 2021;18(6):1607–1609. doi: 10.1038/s41423-021-00679-8.
7. Kather JN, Halama N. Harnessing the innate immune system and local immunological microenvironment to treat colorectal cancer. Br J Cancer. 2019;120(9):871–882. doi: 10.1038/s41416-019-0441-6.
8. Li T-T, Ogino S, Qian ZR. Toll-like receptor signaling in colorectal cancer: carcinogenesis to cancer therapy. World J Gastroenterol. 2014;20(47):17699–17708. doi: 10.3748/wjg.v20.i47.17699.
9. Li T, Cheng H, Yuan H, Xu Q, Shu C, Zhang Y, Xu P, Tan J, Rui Y, Li P, et al. Antitumor activity of cGAMP via stimulation of cGAS-cGAMP-STING-IRF3 mediated innate immune response. Sci Rep. 2016;6(1):19049. doi: 10.1038/srep19049.
10. Chen Y, Shi Y, Wu J, Qi N. MAVS: a two-sided CARD mediating antiviral innate immune signaling and regulating immune homeostasis. Front Microbiol. 2021;12:744348. doi: 10.3389/fmicb.2021.744348.
11. Seth RB, Sun L, Ea C-K, Chen ZJ. Identification and characterization of MAVS, a mitochondrial antiviral signaling protein that activates nf-κB and IRF3. Cell. 2005;122(5):669–682. doi: 10.1016/j.cell.2005.08.012.
12. Ozawa S, Shinohara H, Kanayama H, Bruns CJ, Bucana CD, Ellis LM, Davis DW, Fidler IJ. Suppression of angiogenesis and therapy of human colon cancer liver metastasis by systemic administration of interferon-α. Neoplasia NYN. 2001;3(2):154–164. doi: 10.1038/sj.neo.7900128.
13. Musella M, Galassi C, Manduca N, Sistigu A. The Yin and Yang of type I IFNs in cancer promotion and immune activation. Biology. 2021;10(9):856. doi: 10.3390/biology10090856.
14. Katayama T, Nakanishi K, Nishihara H, Kamiyama N, Nakagawa T, Kamiyama T, Iseki K, Tanaka S, Todo S. Type I interferon prolongs cell cycle progression via p21WAF1/CIP1 induction in human colon cancer cells. Int J Oncol. 2007;31(3):613–620. doi: 10.3892/ijo.31.3.613.
15. Thyrell L, Erickson S, Zhivotovsky B, Pokrovskaja K, Sangfelt O, Castro J, Einhorn S, Grandér D. Mechanisms of interferon-alpha induced apoptosis in malignant cells. Oncogene. 2002;21(8):1251–1262. doi: 10.1038/sj.onc.1205179.
16. O'Donnell JS, Teng MWL, Smyth MJ. Cancer immunoediting and resistance to T cell-based immunotherapy. Nat Rev Clin Oncol. 2019;16(3):151–167. doi: 10.1038/s41571-018-0142-8.
17. Fenton SE, Saleiro D, Platanias LC. Type I and II interferons in the anti-tumor immune response. Cancers. 2021;13(5):1037. doi: 10.3390/cancers13051037.
18. Hwang B-J, Tsao L-C, Acharya CR, Trotter T, Agarwal P, Wei J, Wang T, Yang X-Y, Lei G, Osada T, et al. Sensitizing immune unresponsive colorectal cancers to immune checkpoint inhibitors through MAVS overexpression. J Immunother Cancer. 2022;10(3):e003721. doi: 10.1136/jitc-2021-003721.
19. Pini A, Viti F, Santucci A, Carnemolla B, Zardi L, Neri P, Neri D. Design and use of a phage display library. Human antibodies with subnanomolar affinity against a marker of angiogenesis eluted from a two-dimensional gel. J Biol Chem. 1998;273(34):21769–21776. doi: 10.1074/jbc.273.34.21769.
20. Zhang Z, Liu C, Yang Z, Yin H. CAR-T-Cell therapy for solid tumors positive for fibronectin extra domain B. Cells. 2022;11(18):2863. doi: 10.3390/cells11182863.
21. Baharom F, Ramirez-Valdez RA, Khalilnezhad A, Khalilnezhad S, Dillon M, Hermans D, Fussell S, Tobin KKS, Dutertre C-A, Lynn GM, et al. Systemic vaccination induces CD8+ T cells and remodels the tumor microenvironment. Cell. 2022;185(23):4317–4332.e15. doi: 10.1016/j.cell.2022.10.006.
22. Hauschild A, Gogas H, Tarhini A, Middleton MR, Testori A, Dréno B, Kirkwood JM. Practical guidelines for the management of interferon-α-2b side effects in patients receiving adjuvant treatment for melanoma. Cancer. 2008;112(5):982–994. doi: 10.1002/cncr.23251.
23. Carnemolla B, Neri D, Castellani P, Leprini A, Neri G, Pini A, Winter G, Zardi L. Phage antibodies with pan-species recognition of the oncofoetal angiogenesis marker fibronectin ED-B domain. Int J Cancer. 1996;68(3):397–405. doi: 10.1002/(SICI)1097-0215(19961104)68:3<397:AID-IJC20>3.0.CO;2-4.
24. Castellani P, Viale G, Dorcaratto A, Nicolo G, Kaczmarek J, Querze G, Zardi L. The fibronectin isoform containing the ED-B oncofetal domain: a marker of angiogenesis. Int J Cancer. 1994;59(5):612–618. doi: 10.1002/ijc.2910590507.
25. Neri D, Bicknell R. Tumour vascular targeting. Nat Rev Cancer. 2005;5(6):436–446. doi: 10.1038/nrc1627.
26. Dunn GP, Koebel CM, Schreiber RD. Interferons, immunity and cancer immunoediting. Nat Rev Immunol. 2006;6(11):836–848. doi: 10.1038/nri1961.
27. Parker BS, Rautela J, Hertzog PJ. Antitumour actions of interferons: implications for cancer therapy. Nat Rev Cancer. 2016;16(3):131–144. doi: 10.1038/nrc.2016.14.

28. Kerzel T, Giacca G, Beretta S, Bresesti C, Notaro M, Scotti GM, Balestrieri C, Canu T, Redegalli M, Pedica F, et al. In vivo macrophage engineering reshapes the tumor microenvironment leading to eradication of liver metastases. Cancer Cell. 2023;41(11):1892–1910.e10. doi: 10.1016/j.ccell.2023.09.014.
29. Griswold DP, Corbett TH. A colon tumor model for anticancer agent evaluation. Cancer. 1975;36(6 Suppl):2441–2444. doi: 10.1002/1097-0142(197512)36:6<2441:aid-cncr2820360627>3.0.co;2-p.
30. Corbett TH, Griswold DP, Roberts BJ, Peckham JC, Schabel FM. Tumor induction relationships in development of transplantable cancers of the colon in mice for chemotherapy assays, with a note on carcinogen structure. Cancer Res. 1975;35(9):2434–2439.
31. Moreno BH, Zaretsky JM, Garcia-Diaz A, Tsoi J, Parisi G, Robert L, Meeth K, Ndoye A, Bosenberg M, Weeraratna AT, et al. Response to programmed cell death-1 blockade in a murine melanoma syngeneic model requires costimulation, CD4, and CD8 T cells. Cancer Immunol Res. 2016;4(10):845–857. doi: 10.1158/2326-6066.CIR-16-0060.
32. Castle JC, Loewer M, Boegel S, de Graaf J, Bender C, Tadmor AD, Boisguerin V, Bukur T, Sorn P, Paret C, et al. Immunomic, genomic and transcriptomic characterization of CT26 colorectal carcinoma. BMC Genomics. 2014;15(1):190. doi: 10.1186/1471-2164-15-190.
33. Guo J, Xiao Y, Iyer R, Lu X, Lake M, Ladror U, Harlan J, Samanta T, Tomlinson M, Bukofzer G, et al. Empowering therapeutic antibodies with ifn-α for cancer immunotherapy. PLOS ONE. 2019;14(8):e0219829. doi: 10.1371/journal.pone.0219829.
34. Demaria O, Cornen S, Daëron M, Morel Y, Medzhitov R, Vivier E. Harnessing innate immunity in cancer therapy. Nature. 2019;574(7776):45–56. doi: 10.1038/s41586-019-1593-5.
35. Xie N, Shen G, Gao W, Huang Z, Huang C, Fu L. Neoantigens: promising targets for cancer therapy. Signal Transduct Target Ther. 2023;8(1):1–38. doi: 10.1038/s41392-022-01270-x.
36. Chen K-S, Reinshagen C, Van Schaik TA, Rossignoli F, Borges P, Mendonca NC, Abdi R, Simon B, Reardon DA, Wakimoto H, et al. Bifunctional cancer cell–based vaccine concomitantly drives direct tumor killing and antitumor immunity. Sci Transl Med. 2023;15(677):eabo4778. doi: 10.1126/scitranslmed.abo4778.
37. Reinshagen C, Bhere D, Choi SH, Hutten S, Nesterenko I, Wakimoto H, Le Roux E, Rizvi A, Du W, Minicucci C, et al. Crispr-enhanced engineering of therapy-sensitive cancer cells for self-targeting of primary and metastatic tumors. Sci Transl Med. 2018;10(449):eaao3240. doi: 10.1126/scitranslmed.aao3240.
38. Zhu J-Y, Zheng D-W, Zhang M-K, Yu W-Y, Qiu W-X, Hu J-J, Feng J, Zhang X-Z. Preferential cancer cell self-recognition and tumor self-targeting by coating nanoparticles with homotypic cancer cell membranes. Nano Lett. 2016;16(9):5895–5901. doi: 10.1021/acs.nanolett.6b02786.
39. Dondossola E, Dobroff AS, Marchiò S, Cardó-Vila M, Hosoya H, Libutti SK, Corti A, Sidman RL, Arap W, Pasqualini R. Self-targeting of TNF-releasing cancer cells in preclinical models of primary and metastatic tumors. Proc Natl Acad Sci USA. 2016;113(8):2223–2228. doi: 10.1073/pnas.1525697113.
40. Kim M-Y, Oskarsson T, Acharyya S, Nguyen DX, Zhang X-F, Norton L, Massagué J. Tumor self-seeding by circulating cancer cells. Cell. 2009;139(7):1315–1326. doi: 10.1016/j.cell.2009.11.025.
41. Wen M, Li Y, Qin X, Qin B, Wang Q. Insight into cancer immunity: MHCs, immune cells and commensal microbiota. Cells. 2023;12(14):1882. doi: 10.3390/cells12141882.
42. Seliger B, Wollscheid U, Momburg F, Blankenstein T, Huber C. Characterization of the major histocompatibility complex class I deficiencies in B16 melanoma cells. Cancer Res. 2001;61(3):1095–1099.
43. Accolla RS, Ramia E, Tedeschi A, Forlani G. CIITA-Driven MHC class II expressing tumor cells as antigen presenting cell performers: toward the construction of an optimal anti-tumor vaccine. Front Immunol. 2019;10:10. doi: 10.3389/fimmu.2019.01806.
44. Bou Nasser Eddine F, Forlani G, Lombardo L, Tedeschi A, Tosi G, Accolla RS. Ciita-driven MHC class II expressing tumor cells can efficiently prime naive CD4+ TH cells in vivo and vaccinate the host against parental MHC-II-negative tumor cells. Oncoimmunology. 2016;6(1):e1261777. doi: 10.1080/2162402X.2016.1261777.